Persistent GeV counterpart to the microquasar GRS 1915+105

Guillem Martí-Devesa (D1, 2) and Laura Olivera-Nieto (D3

¹Dipartimento di Fisica, Universitá di Trieste, I-34127 Trieste, Italy
²Istituto Nazionale di Fisica Nucleare, Sezione di Trieste, 34127 Trieste, Italy
³Max-Planck-Institut für Kernphysik, P.O. Box 103980, D 69029, Heidelberg, Germany

ABSTRACT

Microquasars are compact binary systems hosting collimated relativistic jets. They have long been proposed as cosmic-ray accelerators, probed via the gamma-ray emission produced by relativistic particles. However, the observational evidence is steadily increasing but limited: there are around twenty microquasars known to date, of which only three have so far been firmly detected in the GeV gamma-ray range, always in a flaring or special spectral state. Here we present Fermi-LAT observations of the region around the microquasar GRS 1915+105, which reveal the presence of previously unknown multi-GeV emission consistent with the position of the microquasar. No periodicity or variability is found, indicating a persistent source of gamma rays. The properties of the emission are consistent with a scenario in which protons accelerated in the jets interact with nearby gas and produce gamma rays. We find that if the jet has been operating at an average of 1% of the Eddington limit for 10% of the time that GRS 1915+105 spent in its current mass-transfer state, the transfer of 10% of the available power to protons is enough to reach the $\sim 3 \cdot 10^{49}$ erg required to explain the GeV signal. Therefore our results support a scenario in which microquasars with low-mass stellar companions act as hadronic accelerators, strengthening the idea that microquasars as a class contribute to at least some fraction of the observed cosmic-ray flux.

1. INTRODUCTION

Stellar binary systems hosting a compact object reveal themselves through the X-ray emission associated with accretion onto the compact object, earning them the name of X-ray binaries. Microquasars are a subclass of X-ray binaries in which a collimated relativistic outflow of plasma (jet) is formed as a consequence of the aforementioned accretion (Mirabel & Rodríguez 1999; Fender et al. 2004).

The microquasar GRS 1915+105 was first detected as an X-ray source by the WATCH instrument on board of the GRANAT observatory in 1992 (Castro-Tirado et al. 1992). Follow-up observations with the VLA (Mirabel & Rodríguez 1994; Rodríguez & Mirabel 1999) and MERLIN (Fender et al. 1999) in the radio band revealed a highly variable counterpart with apparently superluminal two-sided ejections. This was the first observation of relativistic motions in an object inside our Galaxy, and implied intrinsic velocities for the ejecta near the speed of light. These findings established the presence of a jet with velocity $v \sim 0.8c$ and angle to the line of sight $\theta \sim 63^{\circ}$ (Fender et al. 1999; Rodríguez & Mirabel 1999), making the system a microquasar.

After some initial constraints on the distance by Fender et al. (1999) and Chapuis & Corbel (2004), recent parallax measurements result in a distance estimate of $d = 9.4 \pm 0.6 \pm 0.8$ kpc (Reid & Miller-Jones 2023), which we will adopt through this work.

The mass of the black hole has been subject to debate, with an initial claim of $M_{\rm BH} = 14~\rm M_{\odot}$ (Greiner et al. 2001a) which was later revised to lower values ranging between 10 $\rm M_{\odot}$ (Steeghs et al. 2013) and 12 $\rm M_{\odot}$ (Reid et al. 2014; Reid & Miller-Jones 2023). The corresponding Eddington luminosity is on the order of $\rm L_{Edd} = 1.26\cdot10^{38}\cdot M_{BH}~erg~s^{-1}M_{\odot}^{-1} \sim 10^{39}~erg~s^{-1}$. The spectral type of the donor star was identified to be a K-type star (Greiner et al. 2001b) with a

mass of $0.5M_{\odot}$ (Steeghs et al. 2013), making GRS 1915+105 a low-mass X-ray binary (LMXB). Its orbital period is 33.85 ± 0.16 days (Steeghs et al. 2013).

Since its detection more than 30 years ago, GRS 1915+105 has been extensively monitored from radio to X-ray energies, revealing a highly variable source with distinct behaviours across wavelengths. The emission in the radio band is characterised by quasi-periodic oscillations (Pooley & Fender 1997; Fender & Pooley 2000), seen also in the infrared band (Fender & Pooley 1998). The source flares episodically in both radio and X-rays, with the same anti-correlation between these two bands that is seen for other microquasars. Most notably, GRS 1915+105 had been a consistently bright X-ray source since its discovery, implying intrinsic X-ray luminosities in the range of 0.1 to 1 $L_{\rm Edd}$, until a sudden decrease in June 2018. An initial decrease brought the flux down by an order of magnitude, followed by a continuous decline of the X-ray emission while flaring activity increased at other wavelengths. This behaviour has been attributed to either an obscuration (Motta et al. 2021; Balakrishnan et al. 2021) or an intrinsic change into a hard state (Fender et al. 2004; Koljonen & Hovatta 2021).

Gamma-ray emission from microquasars has long been predicted (e.g. Atoyan & Aharonian 1999; Aharonian 2004; Bosch-Ramon & Khangulyan 2009), both in the high-energy (HE, GeV-scale) and very-high energy (VHE, TeV-scale) bands of the spectrum, usually invoking particle acceleration inside the jets. Only two objects, both high-mass X-ray binaries (HMXB), have so far been firmly detected as GeV sources: Cyg X-3 (Tavani et al. 2009; Fermi LAT Collaboration et al. 2009; Corbel et al. 2012), where orbital gamma-ray modulation is seen and Cyg X-1 (Zanin et al. 2016; Zdziarski et al. 2017), where gamma-ray emission is detected during its hard X-ray state. Additionally, a source has been detected near SS 433 (Li et al. 2020), showing flux variability correlated with the jet precession period. At higher energies only two microquasars have been firmly detected in the VHE band, both as persistent sources: SS 433 (Abeysekara et al. 2018; H. E. S. S. Collaboration et al. 2024; Cao et al. 2024) and the intermediate-mass X-ray binary (IMXB) V4641 Sgr (Albert et al. 2023). No significant VHE emission has been reported from any of the other HE sources (Ahnen et al. 2017; Albert et al. 2021).

In comparison, the gamma-ray detection of LMXBs remains elusive despite intensive searches (particularly during the X-ray flaring states of V404 Cygni; Loh et al. 2016; Piano et al. 2017; Xing & Wang 2021; Harvey et al. 2021). Previous searches for HE emission from GRS 1915+105 placed only flux upper limits (Reimer & Iyudin 2003; Bodaghee et al. 2013). Intriguingly, excess emission was reported by HEGRA at VHE (Aharonian & Heinzelmann 1998), a hint not confirmed by follow-up observations with either the H.E.S.S. (H. E. S. S. Collaboration et al. 2018) or MAGIC (Saito et al. 2009) telescopes.

The relative proximity to Earth of microquasars compared to that of jetted AGNs makes them a critical tool in the study of particle acceleration in jets. However, as every system detected so far displays a unique phenomenology in the gamma-ray band, the role of microquasars as a population remains ambiguous, especially for LMXBs. The recent detection of two systems in the VHE band suggests that microquasars could provide intermittent contributions to the Galactic cosmic-ray sea at energies up to a few PeV (H. E. S. S. Collaboration et al. 2024). However, setting constraints on the magnitude of this contribution remains challenging given the low number of systems detected. Studying the gamma-ray emission from a diverse sample of objects (covering a wide range of jet power, velocity, orientation, and companion mass), is crucial to disentangle the phenomena specific to individual sources from universal properties of particle acceleration in fast-moving jets within our Galaxy.

In this letter we present evidence for a GeV counterpart to the microquasar GRS 1915+105 using the latest Fermi-LAT data, including almost four times as much data as in the latest study dedicated to the same source (Bodaghee et al. 2013). The paper is structured as follows: Section 2 reports on the observation and analysis details; Section 3 presents the results of the spectral, morphological, and flux variability analyses; Section 4 discusses the possible counterparts and evaluates the feasibility of the association with GRS 1915+105; and Section 5 summarises our conclusions.

2. OBSERVATIONS AND ANALYSIS

We use data from the Large Area Telescope (LAT), a pair-production gamma-ray detector onboard the Fermi Gamma-ray Space Telescope (Atwood et al. 2009). The LAT is in operation since August 2008 and thanks to its wide field of view, it surveys the whole sky in photon energies from 30 MeV to more than 100 GeV every 3 h. The LAT's angular resolution depends strongly on the photon energy, with the point-spread function (PSF) 68% containment radius ranging between several degrees at the lowest energies to less than 0.1° above 10 GeV (Abdollahi et al. 2020). To analyse the LAT data we use the Fermitools (v2.2.0; Fermi Science Support Development Team 2019) and fermipy (v1.2.0; Wood et al. 2017) packages.

We select almost 16 years (from August 4 2008 to May 22 2024) of P8R3 SOURCE data (evclass = 128; Atwood et al. 2013; Bruel et al. 2018) from 1 to 100 GeV within 10° of GRS 1915+105. The motivation for the 1 GeV threshold is two-fold: to minimise the impact of the bright diffuse emission in our analysis and take advantage of the improved PSF at higher energies. Additionally, we apply a cut on the zenith angle $z_{\rm max}$ at 105° to prevent Earth-limb contamination. The selected gamma-ray events are binned into a three-dimensional data cube, consisting of a sky-map of dimensions $10^{\circ} \times 10^{\circ}$ (our region of interest, ROI) and 0.04° bin size, centred at the position of GRS 1915+105 and an energy axis with 16 energy bins equally spaced in logarithmic energy between 1 and 100 GeV.

We fit combined spatial and spectral models to this data using a binned maximum-likelihood framework (Mattox et al. 1996). The analysis is done jointly for the PSF0 to PSF3 event types¹. We use the gll_iem_v07.fits and iso_P8R3_SOURCE_V3_PSF3_v1.txt as the Galactic and isotropic diffuse components, respectively, while for the modelling of background sources we employ the 4FGL-DR4 catalogue, adding a component for each source (v34; Abdollahi et al. 2020; Ballet et al. 2023). Energy dispersion correction is applied to all sources except the isotropic diffuse component. In this setup, the detection significance is evaluated considering the test statistic TS = $-2 \ln L_{\text{max},0}/L_{\text{max},1}$, where $L_{\text{max},0}$ is the likelihood value for the null hypothesis and $L_{\text{max},1}$ the likelihood for the tested model. The TS follows a χ^2 distribution, and thus TS = 25 approximately corresponds to a detection at 5σ and 4σ for 1 and 4 source parameters, respectively.

Given the large source density in the region and the addition of substantial data not accounted for in the 4FGL-DR4 catalogue (almost two years), the likelihood fit is performed as follows: (1) we optimise the model of the ROI by fitting the normalisation of all sources in descending order of their predicted number of counts (N_{pred}) down to $N_{\text{pred}} = 1$ (through the fermipy.optimize function). Then, (2) we free the normalisation of all model components within 5° of the centre of the region, and all parameters for those sources within 2.5° or with TS > 500, and fit them with NEWMINUIT. Finally, (3) we search for new sources (> 4σ , > 0.2° from known sources), and refit the ROI repeating step (2). These steps are performed twice to stabilise the fit. The procedure results in three new model components close to GRS 1915+105 not present in the catalogue, required to explain three (> 4σ) gamma-ray excesses in the region. In addition to the TS residual map, we also validate the goodness of our fit through a p-value statistic (PS) data/model deviation estimator (Figure 2, B-C; Bruel 2021). The distribution of this estimator follows the expected distribution ($\propto 10^{-a|x|}$, for which we expected $a \sim 1$ and find a = 1.08), which allows us to conclude that the region is well modelled. This does not mean that all the new model components not present in the catalogue are necessarily of physical origin. For example, they could arise from model defects of the Galactic interstellar emission model (IEM). To address this issue, we perform an additional analysis with gll_iem_v06.fits as an alternative IEM, the diffuse model employed in the latest catalogue of hard GeV sources (3FHL, Ajello et al. 2017). Of the three excesses, shown in Figure 1 and labelled PS J1915.5+1056, PS J1916.6+1051 and PS J1913.4+1050, only the first is detected with TS > 25 regardless of the IEM, suggesting PS J1915.5+1056 is the only excess of astrophysical origin.

3. RESULTS

Here we present a study on PS J1915.5+1056, detected with TS = 33.6 with the standard IEM and TS = 47.9 when using the alternative one. It is best described by a point-like spatial model with best-fit position l, $b = (45.409 \pm 0.026, -0.292 \pm 0.024)$. Interestingly, it is a potential counterpart for GRS 1915+105, as the known microquasar lies at the edge of the source's containment uncertainty $(0.07^{\circ}$ at 99% containment, statistical uncertainty only; Appendix A). Regarding its spectral features, PS J1915.5+1056 is well described with a power law with $\Gamma = 2.25 \pm 0.14$ (Figure 2, A), and an integrated photon flux above 1 GeV of $(6.74 \pm 0.33) \times 10^{-10}$ photons cm⁻² s⁻¹, equivalent to $(3.67 \pm 0.19) \times 10^{-12}$ erg cm⁻² s⁻¹. We do not find significant evidence for curvature (Δ TS = 2.6) nor an exponential cutoff (Δ TS = 3.4) in the spectrum. The quoted uncertainties are statistical only - systematic uncertainties on the flux are mostly dependent on the IEM and of similar amplitude as the statistical uncertainties for standard LAT analyses (Acero et al. 2015).

3.1. Contamination from nearby sources

The region surrounding PS J1915.5+1056 is densely populated by gamma-ray sources and possible counterparts other than GRS 1915+105. We discuss associations with sources known via other wavelengths in Section 4.1. Here we discuss instead the possibility that the new excess is due to poor modelling of one of the known nearby GeV

¹ https://fermi.gsfc.nasa.gov/ssc/data/analysis/documentation/Cicerone/Cicerone_Data/LAT_DP.html

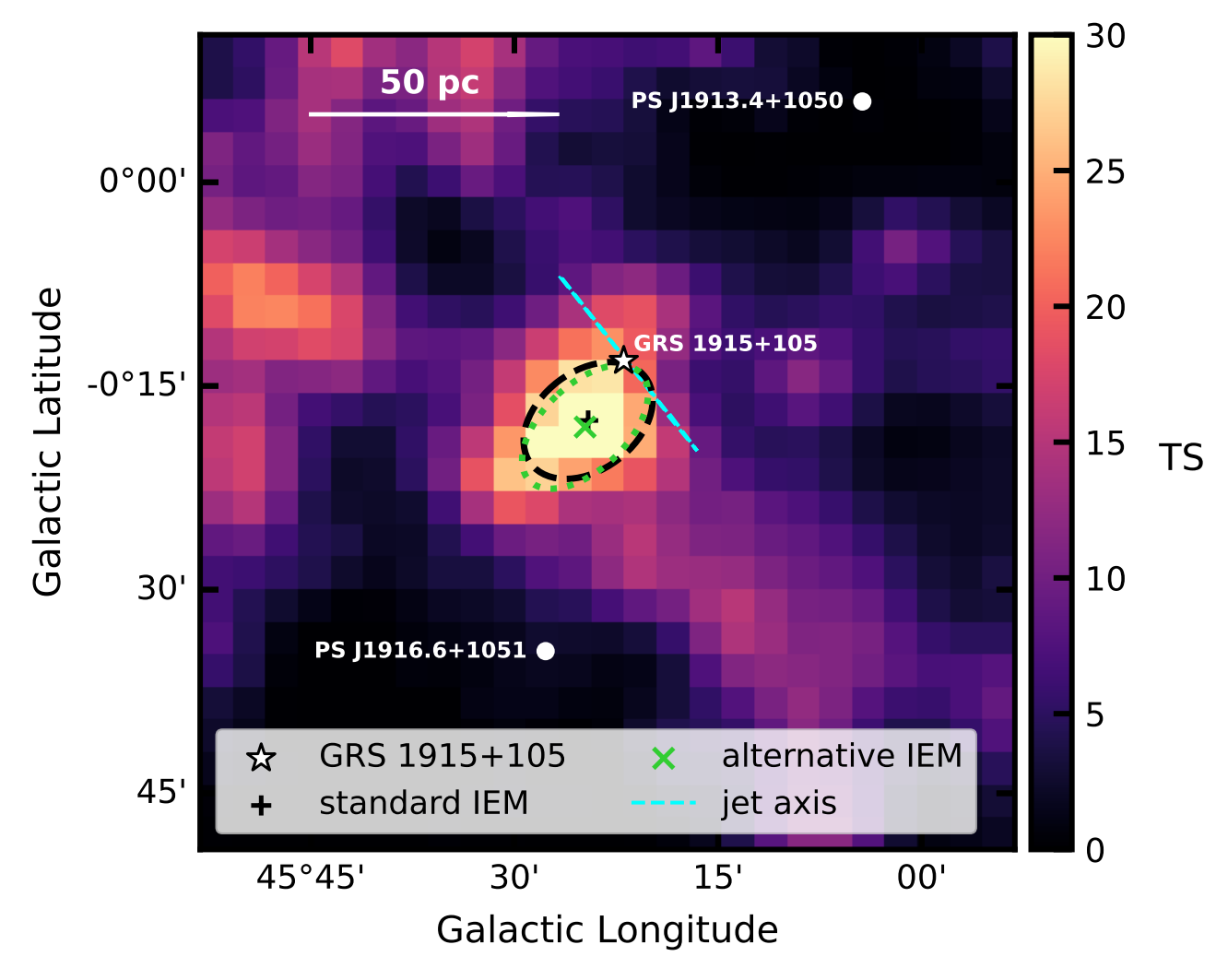


Figure 1. TS residual map (excluding PS J1915.5+1056) of the ROI zoomed to the position of GRS 1915+105, which is marked with a star. The best-fit position and 99% statistical containment region of PS J1915.5+1056 are shown with a cross and dashed black line for the standard IEM and with a cross and dotted green line for the alternative IEM. The other two point-like excesses, which fall below the detection threshold when using the alternative IEM are indicated with white circles. The direction of the jet axis (e.g. Reid et al. (2014)) is indicated with a straight dashed blue line.

sources. In particular, the brightest nearby (< 0.5°) source to PS J1915.5+1056 is 4FGL J1916.3+1108, reported to be the GeV counterpart of the supernova remnant (SNR) G045.7-00.4 (Zhang et al. 2021). We carry out further morphological tests to determine if the GeV excess PS J1915.5+1056 can also be attributed to emission from the SNR when accounting for the spatial extension of the GeV emission from the SNR.

We assess the preference among several morphological models (each with k degrees of freedom) by means of the Akaike information criterion (AIC; Akaike 1998). This is defined as $\Delta \text{AIC} = 2(\Delta k - \Delta \ln L)$. Although the improvement is relatively marginal, the best (i.e. smaller ΔAIC) result is obtained by replacing the point-like spatial model for 4FGL J1916.3+1108 used in the 4FGL-DR4 catalogue with a disk, alongside a point-like component for PS J1915.5+1056 (Table 1). That is, the presence of the new source is preferred even when accounting for the extension of the neighbouring source of $r = 0.23^{+0.14}_{-0.07}$ ($\Delta \text{TS}_{\text{ext}} = 15.14$). This angular size is consistent with the projected size of SNR G045.7-00.4, as well as the results from Zhang et al. (2021). If we further test the extension of PS J1915.5+1056, we derive a limit of 0.14° at 95% confidence ($\Delta \text{TS}_{\text{ext}} = 4.5$). This value increases to 0.22° if instead we consider the 4FGL J1916.3+1108 as a point-like source. The preference for an independent source is additionally supported by an analysis restricted to energies between 5–500 GeV (Appendix A). Consequently, we can confidently state that the new

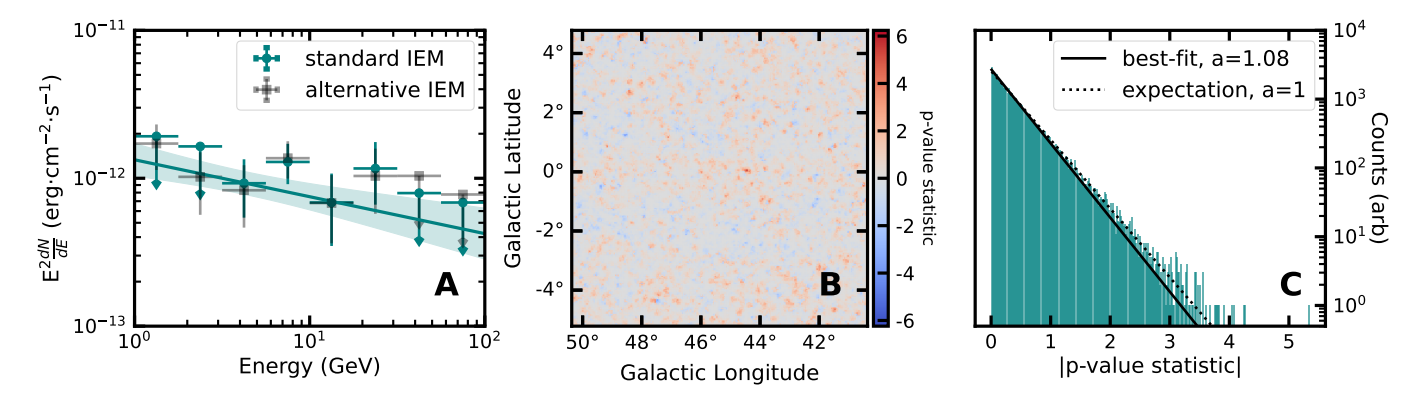


Figure 2. A: Best-fit spectral model and flux points for PS J1915.5+1056. The teal circles show the flux points calculated with the standard IEM and the grey squares correspond to the alternative IEM. Uncertainties are statistical only. The machine-readable values for the flux points shown can be found in Table 2. B: Residual p-value statistic map showing no significant excesses. For reference, PS= 6.24 is equivalent to 5σ . C: Distribution of the residual p-value statistic. The expected distribution is shown with a dotted line, the fitted distribution is shown with a solid line.

Table 1. Likelihood and AIC values for different morphological analyses. The baseline scenario considers the model derived in Section 2 excluding 4FGL J1916.3+1108 and PS J1915.5+1056. The spectrum of 4FGL J1916.3+1108 is always described with a log-parabola shape as in the catalogue. The position of 4FGL J1916.3+1108 is fixed to the catalog value in all steps but the second. The position of PS J1915.5+1056 is always fixed to the one obtained in Section 2. We note that, when PS J1915.5+1056 is not included in the model, the best-fit position of 4FGL J1916.3+1108 is always consistent with the reported 4FGL-DR4 position (< 0.09°, 99% confidence level) and does not shift in the direction of PS J1915.5+1056 regardless of the spatial model considered.

Step	Model	Δk	$\Delta { m AIC}$
0	Baseline	_	_
1	4FGL J1916.3+1108 (point-like, 4FGL-DR4 position)	3	-129.9
2	4FGL J1916.3+1108 (point-like, free position)	5	-129.7
3	4FGL J1916.3+1108 (extended)	6	-168.2
4	4FGL J1916.3+1108 (point-like) + PS J1915.5+1056 (point-like)	9	-153.0
5	4FGL J1916.3+1108 (extended) + PS J1915.5+1056 (point-like, fixed spectrum)	8	-170.1
6	4FGL J1916.3+1108 (extended) + PS J1915.5+1056 (point-like, free spectrum)	10	-169.3

GeV signal is a distinct source, inconsistent in its spatial and spectral properties with other known nearby sources – notably 4FGL J1916.3+1108 ($\Gamma = 3.00 \pm 0.11$), even when considering its extension.

3.2. Search for variability

We further explore the temporal properties of the new gamma-ray source, as these could carry additional information about the underlying particle acceleration processes. To this end, we search for periodical signals and flaring episodes, both blindly and specifically to GRS 1915+105. We employ the likelihood formalism developed by Kerr (2019) and find no significant periodical modulation nor any gamma-ray flares (Appendix B). We also find no significant differences between the emission before and after June 2018, when the system changed its X-ray state. This implies that PS J1915.5+1056 is a persistent gamma-ray source.

4. DISCUSSION

4.1. Identifying the counterpart

There are many classes of astrophysical objects which could be responsible for a point-like GeV excess in the Galactic plane. The most frequent association with point sources in the *Fermi*-LAT data are relatively powerful pulsars (Smith et al. 2023). We make use of the ATNF Pulsar Catalogue (Manchester et al. 2005) and search for known pulsars in the vicinity of the excess. There are 4 pulsars inside a box of 1° width around the excess, three of which have too

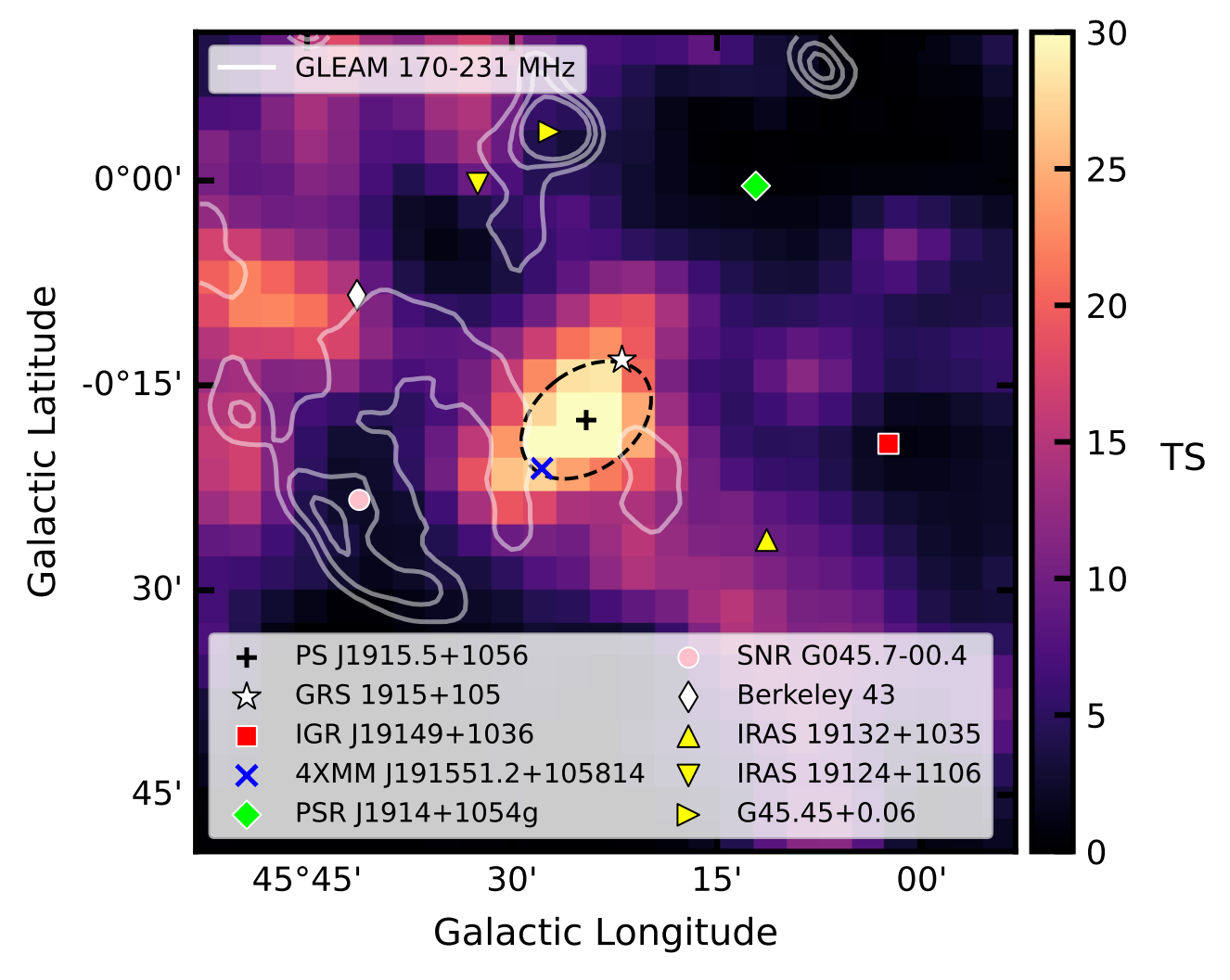


Figure 3. TS map zoomed to the position of PS J1915.5+1056 with the location of possible counterparts. A cross and dashed line represent the best-fit position and 99% containment of PS J1915.5+1056 using the standard IEM. The position of GRS 1915+105 is represented with a white star. The position of the binary IGR J19149+1036 is shown with a red square. The white contours show radio emission from GLEAM (Hurley-Walker et al. 2019) which outline the shape of a nearby SNR, indicated with a pink circle. The closest pulsar and stellar cluster are represented with a green rhombus and a white diamond, respectively. The only source besides GRS 1915+105 which falls within the 99% containment radius is a faint unassociated X-ray source, indicated with a blue x symbol. Finally, the three possible sites of jet interaction with the interstellar medium are indicated with yellow triangles.

low spin-down power values ($\dot{E} < 10^{33} \ {\rm erg \ s^{-1}}$) to account for the excess (Smith et al. 2023). The last object, PSR J1914+1054g, has $\dot{E} = 4 \cdot 10^{35} {\rm erg \ s^{-1}}$ (Motta et al. 2023) but lies more than 0.35° away from the best-fit position (see Figure 3). Given the derived 99% containment radius for the best-fit position is 0.07°, we can rule PSR J1914+1054g out as a likely counterpart.

SNRs can also be bright GeV sources. We query the SNRCat (Ferrand & Safi-Harb 2012) catalogue and find that the only one within the 1° box is SNR G045.7-00.4, which lies 0.3° away from the best-fit position and is already accounted for by existing components in the model. The spectrum of the emission associated with the SNR has a softer spectrum ($\Gamma = 3.00 \pm 0.11$) than the excess ($\Gamma = 2.25 \pm 0.14$), which allows to distinguish them (see Section 3.1). Within a SNR scenario, an asymmetric gamma-ray emission could be accounted for if particles escape from it and interact with nearby dense targets to produce the GeV excess. This has in fact been proposed for another source in the region, 4FGL J1914.5+1107c, whose emission is correlated with dense CO gas at the distance of SNR G045.7-00.4 (Zhang

et al. 2021). However, the CO map at the distance of the SNR shown in Figure 6 of Zhang et al. (2021) reveals no dense target at the location of our GeV excess, ruling out this scenario.

Additionally, several stellar systems within the region could act as particle accelerators. Young (< 10 Myr) stellar clusters (Cassé & Paul 1980; Ackermann et al. 2011; Vieu & Reville 2023) are known to emit photons up to the TeV range, although the emission is usually extended. The closest known nearby cluster is Berkeley 43 (Hunt & Reffert 2023), which is not close enough to account for the excess, at more than 0.3° away from the best-fit position (see Figure 3) with an angular extent of 5 arcminutes. Besides GRS 1915+105, there is another known X-ray binary system in the region of interest, IGR J19149+1036 (Cusumano et al. 2015). The GeV excess exhibits no periodicity following the orbital period of IGR J19149+1036 of 22.25 ± 0.05 days (Figure 5). Furthermore, the binary is located more than 0.35° away from the best-fit position (see Figure 3), so it can be safely discarded as a counterpart.

While the region is filled with possible Galactic counterparts, we also investigate if the GeV signal could arise from an extragalactic source seen through the Galactic plane. There are no known AGN in the region in extragalactic catalogues such as NASA/IPAC or WISE (Assef et al. 2018). However, this is most likely due to the fact that extragalactic catalogues and surveys usually exclude the Galactic Plane (Cook et al. 2023), meaning that the sample of known AGN at low Galactic longitudes is highly biased to the brightest objects. We used the Fermi-LAT fourth catalogue of AGN (4LAC; Ajello et al. 2020) to estimate how many GeV-detectable AGN are expected in our region of interest. There are a total of 2863 objects in the 4LAC catalogue, which only considers high Galactic latitudes ($|b| > 10^{\circ}$). This corresponds to a density of 275.7 objects per steradian, leading to 0.08 GeV-detectable AGN expected within the square of 1° width shown in Figure 3. Taking into account the spectral properties of the observed excess, the expected number of extragalactic sources goes down by a factor of almost 2 (Ajello et al. 2020). We conclude that an extragalactic counterpart is unlikely but cannot at present be fully ruled out.

Finally, the true counterpart could also be an unidentified source. We searched among X-ray catalogues for high-energy sources other than GRS 1915+105 within the GeV 99% containment region. There are none other than GRS 1915+105 in the SRG/ART-XC all-sky catalogue (Sazonov et al. 2024; Pavlinsky et al. 2021), the INTE-GRAL/IBIS 17-year catalogue (Krivonos et al. 2022) and the second release of the *Chandra* catalogue (Evans et al. 2024). In the second *Swift* catalogue 2SXPS, (2SXPS, Evans et al. 2020) there are two sources with good detection quality within the excess error radius - both with the same flux and both at the position of GRS 1915+105, thus they both can be attributed to GRS 1915+105. Finally, in the most recent XMM catalogue (Webb et al. 2020, DR14,) there is one nearby source (besides GRS 1915+105) that passes the good quality flag cut and has a detection likelihood greater than 10. The source is identified as 4XMM J191551.2+105814 (R.A=19:15:51.30, Dec=+10:58:14.7) and it has a flux of $(1.25 \pm 0.19) \cdot 10^{-13}$ erg s⁻¹ cm⁻² in the 0.2 to 12 keV energy range, orders of magnitude below that of GRS 1915+105. No variability is reported for this source. The hardness ratio between the 2-4.5 and 4.5-12 keV bands is 0.1, indicating a relatively soft spectrum. The much fainter and softer X-ray spectrum than GRS 1915+105 suggests a less powerful source and therefore a less likely counterpart – although, again, this possibility cannot be completely excluded.

We conclude that GRS 1915+105 is the favoured counterpart for the new GeV source. In Section 4.2 we discuss a scenario where particles are accelerated in the jets of GRS 1915+105 relatively close to the central binary. Additionally, there have been suggestions that the GRS 1915+105 jets interact with the interstellar medium (ISM) far away from the central binary (Rodriguez & Mirabel 1998; Kaiser et al. 2004; Tetarenko et al. 2018). There are three regions often invoked in this unconfirmed scenario: the two radio sources (IRAS 19132+1035 and IRAS 19124+1106) and the dense HII region G45.45+0.06 (all marked by triangles in Figure 3). We do not detect gamma rays at the location of any of these sources.

4.2. Power requirements

Gamma-ray emission is produced by relativistic particles interacting with their environment. We assume an acceleration region that produces a power-law spectrum of particles $dN/dE \propto E^{-2} \cdot exp(E/E_{\rm cut})$ with a cutoff energy $E_{\rm cut}$ inside the jets of GRS 1915+105 and use the GAMERA code (Hahn 2015; Hahn et al. 2022) to calculate the GeV emission in both a hadronic or leptonic scenario. It is unclear if GRS 1915+105 hosts an alternative source of power such an equatorial outflow (Koljonen & Tomsick 2020), and therefore we do not explore this scenario.

If protons are accelerated to relativistic energies in the jets, they would produce GeV radiation due to inelastic collisions with nearby gas. We use data from the FUGIN ¹²CO (J=1-0) survey based on observations at the Nobeyama Radio Observatory (Umemoto et al. 2017) to determine the density in the region. The details can be found in the

Appendix C. We find values ranging between $18d_{9.4}^{-1}$ and $9d_{9.4}^{-1}$ cm⁻³ depending on the size of the region considered. For a value of the ambient density of $n \sim 18$ cm⁻³, relativistic protons need to reach energies of at least a few hundred GeV ($E_{\rm cut} \gtrsim 250$ GeV) and have a total energy above 1 GeV of $\sim 3\cdot 10^{49}$ erg to match the observed gamma-ray flux. If the average power supplied by the jets is 1% of L_{Edd} and at least 10% of that power (a total of $\sim 10^{36}$ erg s⁻¹) goes to acceleration of cosmic rays, supplying that energy would require ~ 1 Myr. If the lower value of $n \sim 9$ cm⁻³ is considered, this time goes up by a factor two, as it is inversely proportional to the density. Given the estimated duration of the current binary evolution stage of GRS 1915+105 of 10.5 Myr (Belczynski & Bulik 2002), this scenario should in principle be possible, although it is subject to great uncertainty given the unknown real duty cycle of the jets. Once accelerated, the particles would diffuse around the source - how far they can reach depends on value of the diffusion coefficient D. Assuming, as in Khangulyan et al. (2024), an intermediate diffusion regime with $D \sim 10^{26} (E/10 \text{ GeV})^{0.5}$, 200 GeV protons would have reached scales of around 50 pc over one Myr. This corresponds to a 0.3° radius at the distance of GRS 1915+105. Given the slight offset between PS J1915.5+1056 and GRS 1915+105, it is plausible that particles escaped from GRS 1915+105 are causing an enhancement in the cosmic ray density around the source, which then translates to gamma-ray emission only where the target gas is dense enough (Aharonian 2004; Bosch-Ramon et al. 2005; Khangulyan et al. 2024).

If instead we assume the emission to be due to electrons, any consideration is subject to the high uncertainty on the magnetic field and radiation fields in the region. Modelling of the radio properties of GRS 1915+105 suggests a high magnetic field on small scales (< 1 pc from the engine), on the order of 1 G, which would heavily suppress inverse Compton scattering from electrons (Khangulyan et al. 2024). However, the Fermi-LAT results do not tightly constrain the position within the jet. Considering the extension upper limit derived in Section 3, which corresponds to a radius < 36 pc at the distance of GRS 1915+105, the gamma-ray emission could arise from a different region where the magnetic field is considerably lower. Assuming a more favourable value of $B \sim 5\mu G$ on the order of the ISM magnetic field (Jansson & Farrar 2012), the interstellar radiation field from Popescu et al. (2017) at the position of GRS 1915+105 and again an average jet power of 1% of the Eddington luminosity but now with only 1% of this power going to relativistic (> 1 MeV) electrons, an injection time several orders of magnitude longer than the estimated age of GRS 1915+105 of 10.5 Myr (Belczynski & Bulik 2002) would be needed to match the observed gamma-ray flux. One could instead consider an episode in which the accretion rate is higher, which translates to more power carried by the jet and thus available to electrons. Even in such a case, where the jet sustains powers of 10-100% of L_{Edd} , electrons would require 0.1-1\% of that power for at least 10 Myr to match both the observed flux level and spectral index. The prospects for leptonic emission improve if one considers additional sources of radiation such as the companion star or the accretion disk, with the caveat that these will dominate in regions close to the central engine, where the magnetic field might be much higher as well. Note that the combination of assumed magnetic field of $B \sim 5\mu G$ and interstellar radiation field result in faster loss timescales for inverse Compton than synchrotron for the relevant energies. Higher values of $B \sim 10 - 20 \mu G$ such as those estimated at multi-pc scales from other microquasars (Safi-Harb et al. 2022; H. E. S. S. Collaboration et al. 2024) would drive up synchrotron losses and make it even more challenging to explain the GeV observations as inverse Compton emission.

5. CONCLUSION

We have presented here evidence for a GeV counterpart (PS J1915.5+1056) to the microquasar GRS 1915+105. We find a point-like source with a relatively hard spectrum, for which we do not find significant transient or periodic flux modulations. The position of PS J1915.5+1056 is inconsistent with other known potential particle accelerators in the region, and its spectral and morphological properties are sufficiently different from those of the GeV counterpart to the nearby SNR G045.7-00.4 to exclude a common origin. Due to lack of dense gas at the distance of the SNR, we can dismiss the possibility that PS J1915.5+1056 is the result of protons that escaped the SNR. Instead we find that surrounding GRS 1915+105 there is enough gas to explain the observed emission as arising from the interaction of protons accelerated in the jets with the nearby gas. This scenario relies on a moderate duty cycle of the jet power over a relatively large timescale, which is largely unconstrained and subject to great uncertainty. A leptonic scenario is also plausible but disfavoured, as it requires a substantial amount of the jet power, even when assuming a low $(5\mu G)$ magnetic field and the interstellar radiation field as targets for interaction. While we cannot fully discard the association with the much fainter X-ray source 4XMM J191551.2+105814 or an unknown blazar seen through the Galactic plane, we note that there is no evidence for a cutoff in the GeV spectrum of PS J1915.5+1056, which suggests that the emission might extend to even higher gamma-ray energies. A detection in the multi-TeV band would rule

out an extragalactic origin and further confirm the association with GRS 1915+105, particularly given the improved angular resolution of Cherenkov telescopes. The firm identification of this microquasar as a gamma-ray emitter would establish LMXBs as high-energy particle accelerators and constrain their contribution to the cosmic ray content of our Galaxy.

6. ACKNOWLEDGEMENTS

We thank Quentin Remy for his help with the gas density estimation, as well as Jian Li, Teddy Cheung, Matthew Kerr, and Philippe Bruel for their comments on the manuscript. This research has made use of the NASA/IPAC Extragalactic Database, which is funded by the National Aeronautics and Space Administration and operated by the California Institute of Technology. This research has made use of the VizieR catalogue access tool, CDS, Strasbourg, France (Ochsenbein 1996). The original description of the VizieR service was published in Ochsenbein et al. (2000). The CO data were retrieved from the JVO portal (http://jvo.nao.ac.jp/portal/) operated by ADC/NAOJ. The Fermi LAT Collaboration acknowledges generous ongoing support from a number of agencies and institutes that have supported both the development and the operation of the LAT as well as scientific data analysis. These include the National Aeronautics and Space Administration and the Department of Energy in the United States, the Commissariat à l'Energie Atomique and the Centre National de la Recherche Scientifique / Institut National de Physique Nucléaire et de Physique des Particules in France, the Agenzia Spaziale Italiana and the Istituto Nazionale di Fisica Nucleare in Italy, the Ministry of Education, Culture, Sports, Science and Technology (MEXT), High Energy Accelerator Research Organization (KEK) and Japan Aerospace Exploration Agency (JAXA) in Japan, and the K. A. Wallenberg Foundation, the Swedish Research Council and the Swedish National Space Board in Sweden. Additional support for science analysis during the operations phase from the following agencies is also gratefully acknowledged: the Istituto Nazionale di Astrofisica in Italy and the Centre National d'Etudes Spatiales in France. This work performed in part under DOE Contract DE-AC02-76SF00515.

Facilities: Fermi-LAT, Nobeyama Radio Observatory (Umemoto et al. 2017).

Software: astropy (Astropy Collaboration et al. 2013), fermipy (Wood et al. 2017), godot (Kerr 2019), gammapy 1.2 (Donath et al. 2023; Acero et al. 2024), numpy (Harris et al. 2020), matplotlib (Hunter 2007).

APPENDIX

A. ANALYSIS DETAILS

The statistical 99% containment region for the best-fit position when using the standard IEM in the analysis above 1 GeV (see Figure 1) is parameterised as an ellipse with semi-major and semi-minor axes of 0.088° and 0.060° respectively, rotated by an angle 143° with respect to the Galactic North (eastward). For the alternative IEM the values are 0.095°, 0.052° and 136°, respectively. A machine-readable version of the flux points shown in Figure 2 can be found in Table 2.

In order to further verify that PS J1915.5+1056 has different properties than the emission from the nearby SNR, we repeat the analysis with a low energy threshold of 5 GeV. At those energies, PS J1915.5+1056 is still detected at TS = 31, while the TS from 4FGL J1916.3+1108 goes down from TS = 139 to TS = 16. When fitting the region without the additional model component for PS J1915.5+1056, the new best-fit position for 4FGL J1916.3+1108 is found to be at $(l,b) = (45.432 \pm 0.028, -0.298 \pm 0.028)$, and thus consistent only with the position of PS J1915.5+1056 (Appendix A).

B. SEARCH FOR VARIABILITY WITH PHOTON WEIGHTS

We carry out a blind search for state changes by incorporating photon weights into the Bayesian Block algorithm (Scargle et al. 2013; Kerr 2019). Thus, we apply it to the underlying likelihood distribution itself and not to the derived flux points. We select all photons above 100 MeV within 1° of the best-fit position of the source, extending the maximum zenith angle to 105°. The previously derived model ROI is then employed to compute the probability for

Energy	Energy range	Flux	TS	Flux	TS	
		standard	$\operatorname{standard}$	alternative	alternative	
${ m GeV}$	${ m GeV}$	$10^{-12} \text{ erg cm}^{-2} \text{ s}^{-1}$		$10^{-12} \text{ erg cm}^{-2} \text{ s}^{-1}$		
1.33	1-1.78	< 1.922	1.99	1.716 ± 0.587	8.80	
2.37	1.78 - 3.16	< 1.642	2.63	1.022 ± 0.466	4.92	
4.22	3.16 - 5.62	0.925 ± 0.401	6.17	0.830 ± 0.381	5.38	
7.50	5.62 - 10	1.289 ± 0.399	15.42	1.367 ± 0.392	18.81	
13.33	10-17.78	0.686 ± 0.637	5.74	0.680 ± 0.344	6.41	
23.73	17.78 - 31.62	1.165 ± 0.547	9.09	1.036 ± 0.505	8.61	
42.17	31.62 - 56.23	< 0.794	0	< 1.038	0.39	
74.99	56.23-100	< 0.685	0	< 0.777	0	

Table 2. Flux point values for both the standard and alternative diffuse models

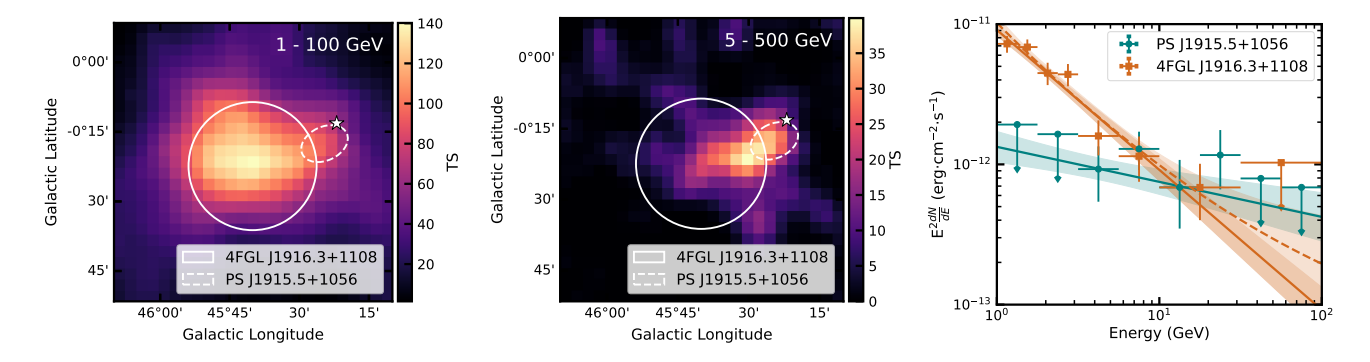


Figure 4. The first two panels show TS residual maps after considering all the model components except those associated with PS J1915.5+1056 and SNR G045.7-00.4, centred at the catalogue position of 4FGL J1916.3+1108. Comparison between the 1–100 GeV (left) and 5–500 GeV (middle) energy ranges reveal energy dependence of the overall morphology of the gamma-ray signal of the region. The solid line represents the best fit extension of 4FGL J1916.3+1108, while the dashed line represents the 99% position uncertainty of PS J1915.5+1056 as obtained in the analysis above 1 GeV (Section 3). The white star represents the nominal position of GRS 1915+105. The remaining panel (right) shows the best-fit spectral model and flux points for the 4FGL J1916.3+1108 power law (solid line) and log-parabola (dashed line) model. The SED of PS J1915.5+1056 (standard IEM case) is also shown for easy comparison.

each photon to be associated with the new source, which is then used as a weight to compute the number of distinct blocks in our light curve (N_b) . We penalise the addition of further blocks by means of a prior $\propto N_b^{\gamma}$. Consequently, the parameter γ sets the significance of flux changes. We derive the false positive rate by redistributing photons randomly among cells (Kerr 2019). In order to ensure zero false detections within the 16 years of data (so, a false alarm rate of 10^{-4}), the prior has to be set to $\gamma = 10$. From this, we find the data to be well represented by a single cell, and therefore the source does not flare significantly (Figure 5). This is consistent with the results by Bodaghee et al. (2013) using 4 years of data. Additionally, we divide the dataset into two ranges: before and after the state change in GRS 1915+105 that occurred in July 1st 2018 (Motta et al. 2021; Balakrishnan et al. 2021). We perform a regular likelihood analysis on each of these ranges, finding no significant distinction between them. Before the state change, the excess has a significance of TS = 23.0 and a flux above 1 GeV of $(3.83 \pm 0.94) \times 10^{-12}$ erg cm⁻² s⁻¹. After the state change the values are TS = 11.4 and $(3.41 \pm 1.19) \times 10^{-12}$ erg cm⁻² s⁻¹ for significance and flux, respectively.

We search for variability that follows the orbital period of GRS 1915+105 by phase-folding the original dataset with said period of (P = 33.85 d, $T_0 = 55458.68$ MJD; Steeghs et al. 2013). We consider 2 and 4 bins of orbital phase and re-fit the model of the ROI with the standard likelihood analysis above 1 GeV as described in Section 2. We find no flux modulation along the orbit. Finally, we employ the previously derived weights to carry out a blind search for periodical modulations by means of a weighted aperture photometry light curve (Fermi LAT Collaboration et al. 2012). We derive the Lomb-Scargle periodogram, shown in Figure 5, which shows no signal in the power distribution

above 3σ . The largest peak is found at the 53.7 d precession period of *Fermi*. No significant period is found either when using the likelihood formalism from Kerr (2019) which considers background periodical fluctuations as well.

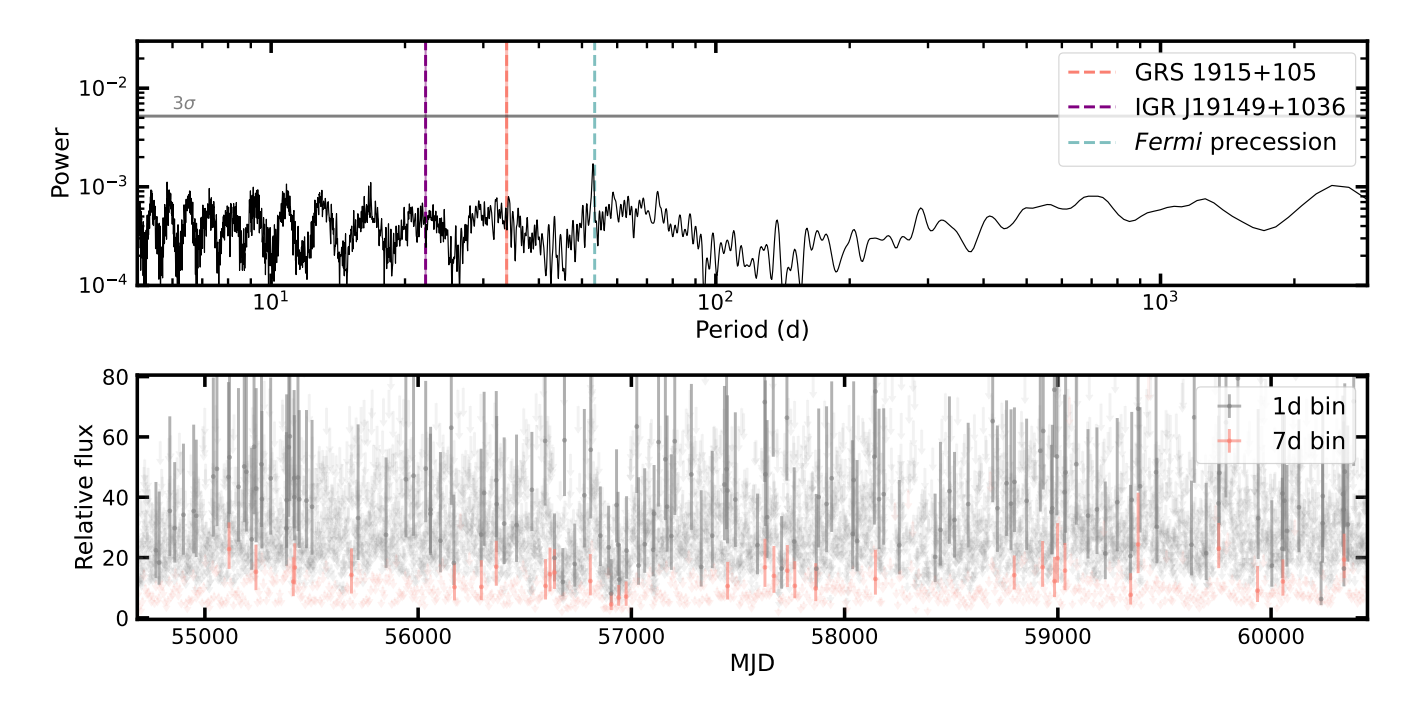


Figure 5. Temporal analysis of PS J1915.5+1056. (Top) Periodogram for PS J1915.5+1056, derived using photon weights. The orbital periods of GRS 1915+105 and IGR J19149+1036 are marked (with the uncertainty represented with a shaded area), as well as Fermi's orbital precession period. Globally, no signal is found above 3σ for any frequency evaluated. (Bottom) Light curve for PS J1915.5+1056 employing a daily and weekly binning. Flux values are displayed relative to that obtained in Section 3. We report detections for bins with TS > 4, otherwise upper limits are reported at 95% confidence level. The results are consistent with a constant flux.

C. ESTIMATION OF THE LOCAL DENSITY

We use data from the FUGIN ¹²CO (J=1-0) survey based on observations at the Nobeyama Radio Observatory (Umemoto et al. 2017) to determine the density in the region. We extract the spectra of ¹²CO in a box with side 0.4° centred on GRS 1915+105. The resulting spectrum is shown in Figure 6 and shows a peak at $V_{LSR} = 26.5 \text{ km s}^{-1}$, which corresponds to a near distance of 1.6 ± 0.4 kpc and a far distance of 10 ± 0.4 kpc (Brand & Blitz 1993; Reid et al. 2019; Wenger et al. 2018; Wenger 2021), the latter consistent with the distance to GRS 1915+105 of $d = 9.4 \pm 0.6 \pm 0.8$ kpc (Reid & Miller-Jones 2023). Note that this peak remains even if the spatial extraction region for the spectra is reduced to a box of side 0.1°. We integrate this peak in each pixel of the box, between velocities of 22.7 and 30 km s⁻¹, which results in the map shown in Figure 6. Adopting a CO-to-H₂ conversion factor X_{CO} following the functional form in Arimoto et al. (1996) and using the same parameters as in CTA Consortium (2023), results in a conversion factor $X_{CO} = 8.45 \cdot 10^{19} \text{ s K}^{-1} \text{ km}^{-1} \text{ cm}^{-2}$ at the distance of GRS 1915+105. Following the procedure outlined in e.g. Miville-Deschênes et al. (2017), we derive a total mass inside of a region of 0.1° radius around the best-fit position of the new GeV source of $1.1 \cdot 10^5 d_{9.4}^2 M_{\odot}$ (within the Fermi-LAT PSF at 10 GeV). Assuming that the mass distribution is homogeneous within a sphere, this corresponds to a hydrogen number density of $n = 19d_{9.4}^{-1}$ cm⁻³. To explore how robust this estimate is, we select a region of the same size around GRS 1915+105, for which the resulting density is $n = 17d_{9.4}^{-1} \text{ cm}^{-3}$. If instead we consider a larger radius corresponding to the extension upper limit of 0.22° (Section 3), the resulting density is lower by a factor 2.

REFERENCES

Abdollahi, S., Acero, F., Ackermann, M., et al. 2020, ApJS, Abeysekara, A. U., Albert, A., Alfaro, R., et al. 2018, Nature, 562, 82, doi: 10.1038/s41586-018-0565-5

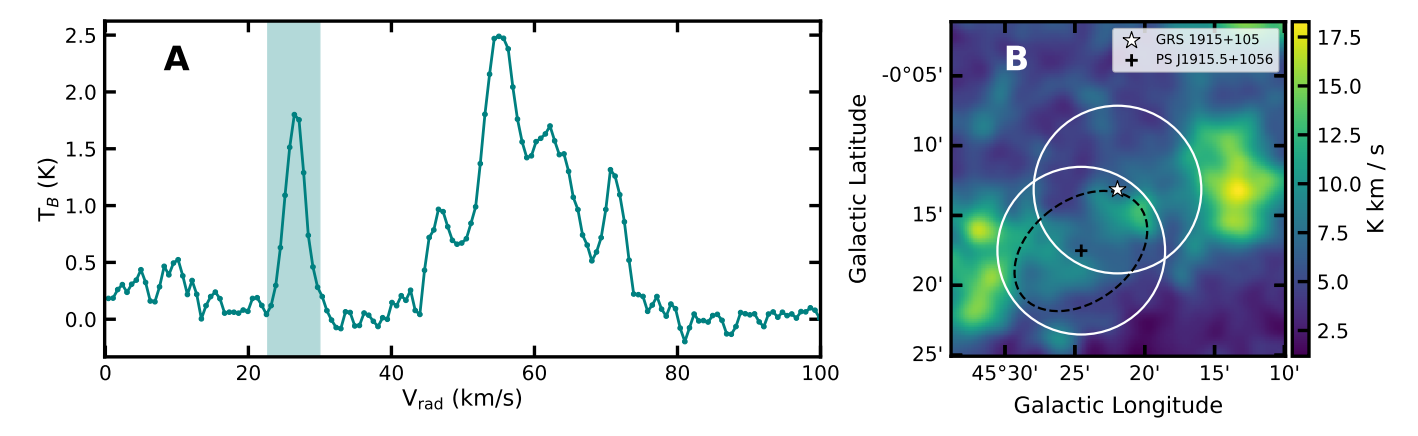


Figure 6. Molecular gas emission around GRS 1915+105. A: FUGIN 12 CO (J=1-0) spectrum of molecular gas towards GRS 1915+105. B: Integrated 12 CO emission map in the velocity interval shaded green in panel A. The white circles represent the extraction regions of 0.1° radius used to derive the number density. The dashed black ellipse and cross show the position and 99% position uncertainty of PS J1915.5+1056. The white star represents the nominal position of GRS 1915+105.

Acero, F., Ackermann, M., Ajello, M., et al. 2015, ApJS, 218, 23, doi: 10.1088/0067-0049/218/2/23

Acero, F., Bernete, J., Biederbeck, N., et al. 2024, Gammapy: Python toolbox for gamma-ray astronomy, v1.2, Zenodo, doi: 10.5281/zenodo.10726484

Ackermann, M., Ajello, M., Allafort, A., et al. 2011, Science, 334, 1103, doi: 10.1126/SCIENCE.1210311/ SUPPL_FILE/ACKERMANN_SOM.PDF

Aharonian, F. A. 2004, Very high energy cosmic gamma radiation: a crucial window on the extreme Universe, doi: 10.1142/4657

Aharonian, F. A., & Heinzelmann, G. 1998, Nuclear Physics B Proceedings Supplements, 60, 193, doi: 10.1016/S0920-5632(97)00514-8

Ahnen, M. L., Ansoldi, S., Antonelli, L. A., et al. 2017, MNRAS, 471, 1688, doi: 10.1093/mnras/stx1690

Ajello, M., Atwood, W. B., Baldini, L., et al. 2017, ApJS, 232, 18, doi: 10.3847/1538-4365/aa8221

Ajello, M., Angioni, R., Axelsson, M., et al. 2020, ApJ, 892, 105, doi: 10.3847/1538-4357/ab791e

Akaike, H. 1998, Information Theory and an Extension of the Maximum Likelihood Principle, ed. E. Parzen,
K. Tanabe, & G. Kitagawa (New York, NY: Springer New York), 199–213, doi: 10.1007/978-1-4612-1694-0_15

Albert, A., Alfaro, R., Alvarez, C., et al. 2021, ApJL, 912, L4, doi: 10.3847/2041-8213/abf35a

Albert, A., Alfaro, R. J., Alvarez, C., et al. 2023, in Proceedings of 38th International Cosmic Ray Conference — PoS(ICRC2023), Vol. 444, 797, doi: 10.22323/1.444.0797

Arimoto, N., Sofue, Y., & Tsujimoto, T. 1996, PASJ, 48, 275, doi: 10.1093/pasj/48.2.275

Assef, R. J., Stern, D., Noirot, G., et al. 2018, ApJS, 234, 23, doi: 10.3847/1538-4365/aaa00a Astropy Collaboration, Robitaille, T. P., Tollerud, E. J., et al. 2013, A&A, 558, A33, doi: 10.1051/0004-6361/201322068

Atoyan, A. M., & Aharonian, F. A. 1999, MNRAS, 302, 253, doi: 10.1046/j.1365-8711.1999.02172.x

Atwood, W., Albert, A., Baldini, L., et al. 2013, arXiv e-prints, arXiv:1303.3514, doi: 10.48550/arXiv.1303.3514

Atwood, W. B., Abdo, A. A., Ackermann, M., et al. 2009, ApJ, 697, 1071, doi: 10.1088/0004-637X/697/2/1071

Balakrishnan, M., Miller, J. M., Reynolds, M. T., et al. 2021, ApJ, 909, 41, doi: 10.3847/1538-4357/abd6cb

Ballet, J., Bruel, P., Burnett, T. H., Lott, B., & The Fermi-LAT collaboration. 2023, arXiv e-prints, arXiv:2307.12546, doi: 10.48550/arXiv.2307.12546

Belczynski, K., & Bulik, T. 2002, ApJL, 574, L147, doi: 10.1086/342480

Bodaghee, A., Tomsick, J. A., Pottschmidt, K., et al. 2013, ApJ, 775, 98, doi: 10.1088/0004-637X/775/2/98

Bosch-Ramon, V., Aharonian, F. A., & Paredes, J. M. 2005, A&A, 432, 609, doi: 10.1051/0004-6361:20041794

Bosch-Ramon, V., & Khangulyan, D. 2009, International Journal of Modern Physics D, 18, 347, doi: 10.1142/S0218271809014601

Brand, J., & Blitz, L. 1993, A&A, 275, 67

Bruel, P. 2021, A&A, 656, A81, doi: 10.1051/0004-6361/202141553

Bruel, P., Burnett, T. H., Digel, S. W., et al. 2018, arXiv e-prints, arXiv:1810.11394,

doi: 10.48550/arXiv.1810.11394

Cao, Z., Aharonian, F., An, Q., et al. 2024, ApJS, 271, 25, doi: 10.3847/1538-4365/acfd29

Cassé, M., & Paul, J. A. 1980, 236C The Astrophysical Journal, 237, 236

- Castro-Tirado, A. J., Brandt, S., & Lund, N. 1992, IAUC, 5590, 2.
 - https://ui.adsabs.harvard.edu/abs/1992IAUC.5590....2C
- Chapuis, C., & Corbel, S. 2004, A&A, 414, 659, doi: 10.1051/0004-6361:20034028
- Cook, D. O., Mazzarella, J. M., Helou, G., et al. 2023, ApJS, 268, 14, doi: 10.3847/1538-4365/acdd06
- Corbel, S., Dubus, G., Tomsick, J. A., et al. 2012, MNRAS, 421, 2947, doi: 10.1111/j.1365-2966.2012.20517.x
- CTA Consortium. 2023, arXiv e-prints, arXiv:2310.02828, doi: 10.48550/arXiv.2310.02828
- Cusumano, G., Segreto, A., La Parola, V., et al. 2015, MNRAS, 446, 1041, doi: 10.1093/mnras/stu2141
- Donath, A., Terrier, R., Remy, Q., et al. 2023, A&A, 678, A157, doi: 10.1051/0004-6361/202346488
- Evans, I. N., Evans, J. D., Martínez-Galarza, J. R., et al. 2024, arXiv e-prints, arXiv:2407.10799. https://arxiv.org/abs/2407.10799
- Evans, P. A., Page, K. L., Osborne, J. P., et al. 2020, ApJS, 247, 54, doi: 10.3847/1538-4365/ab7db9
- Fender, R. P., Belloni, T. M., & Gallo, E. 2004, MNRAS, 355, 1105, doi: 10.1111/j.1365-2966.2004.08384.x
- Fender, R. P., Garrington, S. T., McKay, D. J., et al. 1999, MNRAS, 304, 865, doi: 10.1046/j.1365-8711.1999.02364.x
- Fender, R. P., & Pooley, G. G. 1998, MNRAS, 300, 573, doi: 10.1046/j.1365-8711.1998.01921.x
- —. 2000, MNRAS, 318, L1,
 - doi: 10.1046/j.1365-8711.2000.03847.x
- Fermi LAT Collaboration, Abdo, A. A., Ackermann, M., et al. 2009, Science, 326, 1512, doi: 10.1126/science.1182174
- Fermi LAT Collaboration, Ackermann, M., Ajello, M., et al. 2012, Science, 335, 189, doi: 10.1126/science.1213974
- Fermi Science Support Development Team. 2019, Fermitools: Fermi Science Tools, Astrophysics Source Code Library, record ascl:1905.011. http://ascl.net/1905.011
- Ferrand, G., & Safi-Harb, S. 2012, Advances in Space Research, 49, 1313, doi: 10.1016/j.asr.2012.02.004
- Greiner, J., Cuby, J. G., & McCaughrean, M. J. 2001a, Nature, 414, 522, doi: 10.1038/35107019
- Greiner, J., Cuby, J. G., McCaughrean, M. J., Castro-Tirado, A. J., & Mennickent, R. E. 2001b, A&A, 373, L37, doi: 10.1051/0004-6361:20010771
- H. E. S. S. Collaboration, Abdalla, H., Abramowski, A., et al. 2018, A&A, 612, A10, doi: 10.1051/0004-6361/201527773
- H. E. S. S. Collaboration, Aharonian, F., Ait Benkhali, F., et al. 2024, Science, 383, 402, doi: 10.1126/science.adi2048

- Hahn, J. 2015, in International Cosmic Ray Conference, Vol. 34, 34th International Cosmic Ray Conference (ICRC2015), 917.
 - https://ui.adsabs.harvard.edu/abs/2015ICRC...34..917H
- Hahn, J., Romoli, C., & Breuhaus, M. 2022, GAMERA: Source modeling in gamma astronomy, Astrophysics Source Code Library, record ascl:2203.007. http://ascl.net/2203.007
- Harris, C. R., Millman, K. J., van der Walt, S. J., et al. 2020, Nature, 585, 357, doi: 10.1038/s41586-020-2649-2
- Harvey, M., Rulten, C. B., & Chadwick, P. M. 2021, MNRAS, 506, 6029, doi: 10.1093/mnras/stab2097
- Hunt, E. L., & Reffert, S. 2023, A&A, 673, A114, doi: 10.1051/0004-6361/202346285
- Hunter, J. D. 2007, Computing in Science & Engineering, 9, 90, doi: 10.1109/MCSE.2007.55
- Hurley-Walker, N., Hancock, P. J., Franzen, T. M. O., et al. 2019, PASA, 36, e047, doi: 10.1017/pasa.2019.37
- Jansson, R., & Farrar, G. R. 2012, ApJ, 757, 14, doi: 10.1088/0004-637X/757/1/14
- Kaiser, C. R., Gunn, K. F., Brocksopp, C., & Sokoloski, J. L. 2004, ApJ, 612, 332, doi: 10.1086/422466
- Kerr, M. 2019, ApJ, 885, 92, doi: 10.3847/1538-4357/ab459f Khangulyan, D., Bosch-Ramon, V., & Hadasch, D. 2024,
 - Journal of High Energy Astrophysics, 43, 93, doi: 10.1016/j.jheap.2024.06.006
- Koljonen, K. I. I., & Hovatta, T. 2021, A&A, 647, A173, doi: 10.1051/0004-6361/202039581
- Koljonen, K. I. I., & Tomsick, J. A. 2020, A&A, 639, A13, doi: 10.1051/0004-6361/202037882
- Krivonos, R. A., Sazonov, S. Y., Kuznetsova, E. A., et al. 2022, MNRAS, 510, 4796, doi: 10.1093/mnras/stab3751
- Li, J., Torres, D. F., Liu, R.-Y., et al. 2020, Nature Astronomy, 4, 1177, doi: 10.1038/s41550-020-1164-6
- Loh, A., Corbel, S., Dubus, G., et al. 2016, MNRAS, 462, L111, doi: 10.1093/mnrasl/slw142
- Manchester, R. N., Hobbs, G. B., Teoh, A., & Hobbs, M. 2005, AJ, 129, 1993, doi: 10.1086/428488
- Mattox, J. R., Bertsch, D. L., Chiang, J., et al. 1996, ApJ, 461, 396, doi: 10.1086/177068
- Mirabel, I. F., & Rodríguez, L. F. 1994, Nature, 371, 46, doi: 10.1038/371046a0
- —. 1999, ARA&A, 37, 409, doi: 10.1146/annurev.astro.37.1.409
- Miville-Deschênes, M.-A., Murray, N., & Lee, E. J. 2017, ApJ, 834, 57, doi: 10.3847/1538-4357/834/1/57
- Motta, S. E., Turner, J. D., Stappers, B., et al. 2023, MNRAS, 523, 2850, doi: 10.1093/mnras/stad1438
- Motta, S. E., Kajava, J. J. E., Giustini, M., et al. 2021, MNRAS, 503, 152, doi: 10.1093/mnras/stab511

- Ochsenbein, F. 1996, The VizieR database of astronomical catalogues, CDS, Centre de DonnA©es astronomiques de Strasbourg, doi: 10.26093/CDS/VIZIER
- Ochsenbein, F., Bauer, P., & Marcout, J. 2000, A&AS, 143, 23, doi: 10.1051/aas:2000169
- Pavlinsky, M., Tkachenko, A., Levin, V., et al. 2021, A&A, 650, A42, doi: 10.1051/0004-6361/202040265
- Piano, G., Munar-Adrover, P., Verrecchia, F., Tavani, M., & Trushkin, S. A. 2017, ApJ, 839, 84, doi: 10.3847/1538-4357/aa6796
- Pooley, G. G., & Fender, R. P. 1997, MNRAS, 292, 925, doi: 10.1093/mnras/292.4.925
- Popescu, C. C., Yang, R., Tuffs, R. J., et al. 2017, MNRAS, 470, 2539, doi: 10.1093/mnras/stx1282
- Reid, M. J., McClintock, J. E., Steiner, J. F., et al. 2014, ApJ, 796, 2, doi: 10.1088/0004-637X/796/1/2
- Reid, M. J., & Miller-Jones, J. C. A. 2023, ApJ, 959, 85, doi: 10.3847/1538-4357/acfe0c
- Reid, M. J., Menten, K. M., Brunthaler, A., et al. 2019, ApJ, 885, 131, doi: 10.3847/1538-4357/ab4a11
- Reimer, O., & Iyudin, A. 2003, in International Cosmic Ray Conference, Vol. 4, International Cosmic Ray Conference, 2341
- Rodriguez, L. F., & Mirabel, I. F. 1998, A&A, 340, L47, doi: 10.48550/arXiv.astro-ph/9811250
- Rodríguez, L. F., & Mirabel, I. F. 1999, ApJ, 511, 398, doi: 10.1086/306642
- Safi-Harb, S., Mac Intyre, B., Zhang, S., et al. 2022, ApJ, 935, 163, doi: 10.3847/1538-4357/ac7c05
- Saito, T. Y., Zanin, R., Bordas, P., et al. 2009, arXiv e-prints, arXiv:0907.1017, doi: 10.48550/arXiv.0907.1017
- Sazonov, S., Burenin, R., Filippova, E., et al. 2024, A&A, 687, A183, doi: 10.1051/0004-6361/202348950

- Scargle, J. D., Norris, J. P., Jackson, B., & Chiang, J. 2013, ApJ, 764, 167, doi: 10.1088/0004-637X/764/2/167
- Smith, D. A., Abdollahi, S., Ajello, M., et al. 2023, ApJ, 958, 191, doi: 10.3847/1538-4357/acee67
- Steeghs, D., McClintock, J. E., Parsons, S. G., et al. 2013, ApJ, 768, 185, doi: 10.1088/0004-637X/768/2/185
- Tavani, M., Bulgarelli, A., Piano, G., et al. 2009, Nature, 462, 620, doi: 10.1038/nature08578
- Tetarenko, A. J., Freeman, P., Rosolowsky, E. W., Miller-Jones, J. C. A., & Sivakoff, G. R. 2018, MNRAS, 475, 448, doi: 10.1093/mnras/stx3151
- Umemoto, T., Minamidani, T., Kuno, N., et al. 2017, PASJ, 69, 78, doi: 10.1093/pasj/psx061
- Vieu, T., & Reville, B. 2023, MNRAS, 519, 136, doi: 10.1093/mnras/stac3469
- Webb, N. A., Coriat, M., Traulsen, I., et al. 2020, A&A, 641, A136, doi: 10.1051/0004-6361/201937353
- Wenger, T. 2021, tvwenger/kd: v2.1, Zenodo, doi: 10.5281/ZENODO.5660905
- Wenger, T. V., Balser, D. S., Anderson, L. D., & Bania, T. M. 2018, ApJ, 856, 52, doi: 10.3847/1538-4357/aaaec8
- Wood, M., Caputo, R., Charles, E., et al. 2017, in International Cosmic Ray Conference, Vol. 301, 35th International Cosmic Ray Conference (ICRC2017), 824, doi: 10.22323/1.301.0824
- Xing, Y., & Wang, Z. 2021, ApJ, 922, 111, doi: 10.3847/1538-4357/ac25fd
- Zanin, R., Fernández-Barral, A., de Oña Wilhelmi, E., et al. 2016, A&A, 596, A55, doi: 10.1051/0004-6361/201628917
- Zdziarski, A. A., Malyshev, D., Chernyakova, M., & Pooley, G. G. 2017, MNRAS, 471, 3657, doi: 10.1093/mnras/stx1846
- Zhang, H.-M., Liu, R.-Y., Su, Y., et al. 2021, ApJ, 923, 106, doi: 10.3847/1538-4357/ac36c6